PIN: PROLATE SPHEROIDAL WAVE FUNCTION-BASED IMPLICIT NEURAL REPRESENTATIONS

Anonymous authors
Paper under double-blind review

ABSTRACT

Implicit Neural Representations (INRs) provide a continuous mapping between the coordinates of a signal and the corresponding values. As the performance of INRs heavily depends on the choice of nonlinear-activation functions, there has been a significant focus on encoding explicit signals within INRs using diverse activation functions. Despite recent advancements, existing INRs often encounter significant challenges, particularly at fine scales where they often introduce noise-like artifacts over smoother areas compromising the quality of the output. Moreover, they frequently struggle to generalize to unseen coordinates. These drawbacks highlight a critical area for further research and development to enhance the robustness and applicability of INRs across diverse scenarios. To address this challenge, we introduce the **P**rolate Spheroidal Wave Function-based **I**mplicit **N**eural Representations (PIN), which exploits the optimal space-frequency domain concentration of Prolate Spheroidal Wave Functions (PSWFs) as the nonlinear mechanism in INRs. Our experimental results reveal that PIN excels not only in representing images and 3D shapes but also significantly outperforms existing methods in various vision tasks that require INR generalization, including image inpainting, novel view synthesis, edge detection, and image denoising.

1 INTRODUCTION

Discrete representations of images and shapes currently dominate computer vision tasks, with benefits derived from their convenience in storage and computation. Nonetheless, it is worth noting that memory consumption escalates exponentially with the dimensions and resolutions of the data. Moreover, the discrete formation limits the expressivity with the finite discrete grid size or volume size. Implicit Neural Representation (INR) (Sitzmann et al., 2020; Tancik et al., 2020) provides an alternative mechanism that continuously represents signals parameterized through Multi-layer Perceptions (MLPs). INRs are usually fully connected neural networks designed to learn a continuous mapping between coordinates of a signal to the corresponding signal values, resulting in a compact representation of the signal with arbitrary resolution. Beyond representation (Chen et al., 2023b; Saragadam et al., 2022), INRs have demonstrated prominent advantages in various vision tasks, including image reconstruction (Czerkawski et al., 2021; Saragadam et al., 2023), medical imaging (Shen et al., 2022; Sun et al., 2021), and novel view synthesis (Barron et al., 2021; Mildenhall et al., 2020; Niemeyer et al., 2020).

Despite the evident advantages delineated above for INRs in vision computing tasks, properties of some inherent structures of INRs present obstacles to a more widespread application in various vision tasks. First, the expressivity of INRs is heavily influenced by the choice of activation function (Sitzmann et al., 2020; Ramasinghe & Lucey, 2022; Saragadam et al., 2023). The original INRs employing ReLU as activation function were demonstrated to exhibit poor performance in signal representation tasks due to the spectral bias of MLPs (Basri et al., 2020; Rahaman et al., 2019), which favors learning low-frequency and lacks the ability to represent fine details. Also, when reconstructing from sparse measurements, INRs tend to overfit to the coordinates used during training, i.e., the INR can only accurately represent the signal values of the trained coordinates, leading to blurry or noisy reconstructions.

Fourier features (Tancik et al., 2020) or positional encoding (Mildenhall et al., 2020) is a transformation which maps low-dimensional coordinates to high-dimensional features, enabling MLP's

input layer to embed high frequencies and learning the high-frequency content of a signal (Tancik et al., 2020). Several alternative nonlinearities including sinusoids (Sitzmann et al., 2020), Gaussian functions (Ramasinghe & Lucey, 2022), and Gabor Wavelets (Saragadam et al., 2023) have been proposed as replacements for ReLUs along with positional embedding schemes, often leading to notable enhancements in signal encoding capabilities. One key property of Gaussians and Gabor Wavelets is their good balance of joint space-frequency energy concentration, which explains their efficient performance according to classical signal p rocessing. Nevertheless, another limitation of current INR design is their high sensitivity to hyperparameter selection of parameters. Gaussian and Gabor wavelet nonlinearities require to set a predefined frequency or scale parameter for the INR to achieve competitive performance. How to determine best hyperparameters for the INR activation function and how to initialize the network is still heuristic, and highly dependent on the processing task.

Numerous recent studies have explored the inherent properties of INRs through theoretical analyses and experimental investigations to advance the understand of the mechanisms behind their success and limitations. The Neural Tangent Kernel (NTK) (Jacot et al., 2018) was used to reveal that standard MLP converges very slowly to high-frequency signals in low-dimensional coordinate-based INRs, owing to the rapid frequency fall-off of its corresponding kernels.When utilizing Fourier features (Tancik et al., 2020) or sinusoidal activation functions (Sitzmann et al., 2020) or their recently introduced variants (Liu et al., 2024; Shi et al., 2024; Kazerouni et al., 2024), which aim to achieve superior representation through variable periodic activation functions, sinusoid adjustments based on deep prior knowledge, and Fourier reparameterization, respectively, the Neural Tangent Kernel (NTK) is transformed into a stationary (shift-invariant) kernel, enabling control over the range of learned frequencies (Tancik et al., 2020). The work by Yüce et al. (2022) provided a theoretical analysis of the expressivity and inductive bias of INRs, as well as the imperfect recovery resulting from the inadequacy of input frequencies to properly capture the frequency of the signal. Experimentally, Saragadam et al. (2023) investigated the first l ayer o utput o f I NR, d emonstrating that the spatial and frequency compactness of the activation function, as well as the multi-dimensional non-linearity, provide more accurate representations for natural images. Roddenberry et al. (2023) demonstrated that the output of an INR with a generic wavelet activation in the first l ayer c an be expressed in terms of the same wavelets.

In this paper, motivated by these recent theoretical and experimental findings, we propose the employment of a novel activation function for INRs: the Prolate Spheroidal Wave Function (PSWF). PSWFs are designed to maximize the spatial and frequency domain energy concentration, and have previously been used in many vision applications (Lindquist & Wager, 2008; Wendt et al., 2010; Brown & DC, 1968) demonstrating that having an optimal balance of energy concentration in both spatial and frequency domains is critical for efficient signal representation and approximation (Ramasinghe & Lucey, 2022; Saragadam et al., 2023). Our results below showcase that emplying PSWFs as the activation function for INRs endows this architecture with greater expressivity and generalizability as compared to sinusoidal, Gaussian, and Gabor functions which are currently used in state-of-the-art INR implementations. *We attribute this improved performance to the high energy compactification of PSWF atoms and their flexibility, namely the ability to easily tune their hyperparameters to various tasks*. Extensive numerical experiments demonstrate that our new INR model excels not only in representation tasks but also in more challenging reconstruction tasks, e.g., image inpainting, where exisitng INRs often perform poorly.

2 Related works

Implicit Neural Representation. INRs have emerged in recent years showcasing remarkable performances not only in signal representation tasks but also in many inverse vision applications, e.g., unordered signal representation such as 3D shape representation (Park et al., 2019; Mescheder et al., 2019) or novel-view synthesis (Barron et al., 2021; Mildenhall et al., 2020; Niemeyer et al., 2020). The INR represents signals by parameterizing the mappings between input coordinates and signal values using an MLP. The MLP usage here differs from the standard approach in that the inputs are low-dimensional coordinates instead of high-dimensional pixels. In such cases, the ReLU activation function performs poorly due to its *spectral bias*. Recent works have improved the expressivity of INRs by incorporating coordinate transformation or introducing a special type of non-linearity for the MLP, resulting in enhanced performance in signal representation tasks. Unlike conventional

neural networks, the training of INRs is always conducted on a case-by-case basis, which hinders their widespread adoption in vision computing tasks. Several works have proposed accelerating training through multi-scale methods (Saragadam et al., 2022), local blocks (Reiser et al., 2021), Mixture-of-Expert (Wang et al., 2022), adaptive coordinate (Martel et al., 2021).

Expressivity of INRs. Despite the widespread adoption of INRs in various tasks, a thorough theoretical understanding is still limited. Fourier analysis was used to explore the *spectral bias* of standard MLPs with ReLU (Rahaman et al., 2019; Cao et al., 2019; Basri et al., 2020), i.e. low frequency is learning fast and robust to noise. The use of Fourier Feature Network (FFN) (Tancik et al., 2020) or periodic non-linearity (SIREN) (Sitzmann et al., 2020) can alleviate spectral bias by transforming the NTK to a stationary (shift-invariant) kernel. Building upon the basic property of trigonometric function, Yüce et al. (2022) demonstrated that the expressivity of FFN and SIREN essentially share the same expressive power, which is characterized by the linear combination of sinusoidal functions at integer hamonics. They also identified the reason for the failure recovery as resulting from the uncovered spectral components, which leads to severe artifacts. For non-periodic activations, such as wavelet (Saragadam et al., 2023),Roddenberry et al. (2023) derived a bound of functions that can be represented by INR.

3 METHODOLOGY

3.1 FORMULATION OF AN INR

An INR encodes the mapping between input coordinates $\mathbf{r} \in \mathbb{R}^I$ and corresponding signal values $f(\mathbf{r}) \in \mathbb{R}^O$, denoted as $g : \mathbb{R}^I \to \mathbb{R}^O$, and the mapping ,which is g, is parameterized by a fully connected neural network $\Phi_\theta : \mathbb{R}^I \to \mathbb{R}^O$, where θ represents the parameters of the neural network. For instance, when representing an image, the INR maps pixel coordinates $\mathbf{r} = (x_i, y_i)$ to the corresponding RGB values $f(\mathbf{r}) = (R_i, G_i, B_i)$. The fully connected network Φ_θ typically an L layer MLP, each layer given by:

$$\begin{aligned} \boldsymbol{z}_0 &= \gamma(\boldsymbol{r}) \\ \boldsymbol{z}_k &= \sigma(\boldsymbol{W}_k \boldsymbol{z}_{k-1} + \boldsymbol{b}_k)), k = 1, \ldots, L-1 \\ \boldsymbol{z}_L &= \boldsymbol{W}_L \boldsymbol{z}_{L-1} + \boldsymbol{b}_L. \end{aligned} \tag{1}$$

where γ is the position encoding, σ is the nonlinear activation function. $\boldsymbol{W}_k$, $\boldsymbol{b}_k$ are weights and biases of the k'th layer. $\boldsymbol{z}_0 \in \mathbb{R}^I$ is the input coordinate and $\boldsymbol{z}_L \in \mathbb{R}^O$ is the output of final layer.

3.2 WHY PSWFS?

In the recent INR literature, periodic functions such as the sinusoidal activation function and its analogous Fourier embedding have shown to yield better approximations than ReLU, particularly for reconstructing high-frequency components. Functions with better spatial localization, such as Gaussian (Ramasinghe & Lucey, 2022) or Gabor wavelets (Saragadam et al., 2022) have shown higher accuracy in image and shape representation tasks, benefiting from their analytic properties. Even though INRs with these activations work competitively in image and shape representation problems, they work poorly for reconstruction tasks from sparse or noisy measurements, such as image inpainting and denoising. Furthermore, when encoding the signals, existing INRs have a tendency to lose the balance between smoother and finer detailed areas in favor of finer details. A reason for these limitations could be the inadequate energy compactification of INRs when employing Gabor wavelets or Gaussians. This problem is demonstrated by the great sensitivity of INRs to the selection of scale and frequency parameters for Gaussians and Gabor wavelets (Saragadam et al., 2023). Signal representation can be improved by adjusting these parameters for each signal to make such activations more compact in space. However, fine tuning those parameters from signal to signal is extremely tardy, and inefficient task. In addition to that, when INRs are trained on partial data and evaluated on the entire dataset, they fail to generalize, even with different parameter settings. The recovered-masked areas tend to be purely noisy. Similarly, in image denoising, the INRs tend to learn the noise, making it difficult to remove effectively. These observations motivate us to explore alternate activation functions with better space-frequency compactification and lead to PSWFs. Figure 1 shows the space-frequency trade-off of the existing activations along with PSWF.

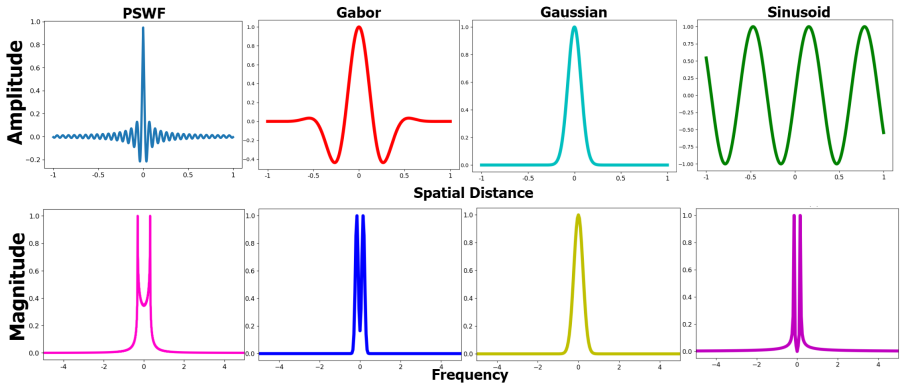

Figure 1: **Space-Frequency Tradeoff of Activations**: The top row illustrates how the values of activation functions change with spatial distance, while the bottom row demonstrates how their magnitudes vary in the Fourier domain with frequency. When an activation function compresses in the spatial domain, it tends to have a broader spectrum in the frequency domain, and vice versa. This phenomenon is known as the space-frequency tradeoff of functions. PSWFs are recognized for their optimality in preserving the highest energy across both domains.

3.3 Prolate Spheroidal Wave Functions

PSWFs originated from a question posed by Shannon (Moore & Cada, 2004) in the 1960s: *To what extent are functions, which are confined to a finite bandwidth, also concentrated in the time domain?* Slepian (Slepian & Pollak, 1961; Slepian, 1964; Landau & Pollak, 1961b; 1962), discovered that such functions are associated with the solutions to a Sturm-Liouville problem arising from the Helmholz equation on the prolate sphere (hence the name). In a seminal sequence of papers, Slepian, Pollak and Landau at Bell Labs introduced an integral formulation for this energy concentration problem which led to the following equation (Landau & Pollak, 1961a; Slepian & Pollak, 1961) where the PSWFs $\psi_n(c,t)$ are the eigenfunction solution of the integral operator problem

$$\int_{-t_0}^{t_0} \psi_n(c,t) \frac{\sin \Omega(x-t)}{\pi(x-t)} \mathrm{d}t = \psi_n(c,x)\lambda_n(c),$$

where $\lambda_n(c)$ are corresponding eigenvalues, c is the bandwidth parameter and $c = t_0\Omega$, Ω is the cut-off frequency of $\lambda_n(c)$. The PSWFs form an orthonormal basis of the space of Ω-bandlimited functions with the fundamental property of being maximally concentrated in time and frequency domain. This energy concentration property has been proven to very advantageous in various signal processing tasks (Gosse, 2013; Hu et al., 2014; Lindquist & Wager, 2008), most notably in sampling problems where PSWFs have been employed for image reconstruction from sparse samples (Khare & George, 2003; Hogan et al., 2010; Lindquist, 2003). The success of PSWFs in sampling applications is of particular interest here, as it suggests their potential for efficiently representing complex information. In our results section below, we confirm that leveraging excellent expressivity properties with robustness in the sparse and possibly noisy sampling setting; PSWFs leads to a remarkably effective choice of activation function for INRs.

In an INR model that employs polynomial activation functions and compactly supported wavelets as template functions in the first layer, Roddenberry et al. (2023) demonstrates that the Fourier transform of the INR output can be characterized by the convolutions of the Fourier transforms of the first-layer atoms with themselves. This observation can be extended to PSWFs which have not compact support but have rapid space decay. They are a generalization of Legendre polynomials and can be represented by the expansion:

$$\psi_n(c,t) = \sum_{k=0}^{\infty} \beta_k^n P_k(t), \tag{2}$$

where $P_k(t)$ is normalized version of Legendre polynomial of order k where the coefficients β_k can be calculated by recurrence relation as shown in Moore & Cada (2004).

As shown in Roddenberry et al. (2023) and Yüce et al. (2022), the support of scaled and shifted versions of the template in the first layer is preserved, implying that the output at given coordinate relies solely on the template in the first layer whose support contains this coordinate. For PSWFs it is indeed true that the Fourier support is preserved. As a result, the Fourier output at a given coordinate ξ is dependent only upon the PSWFs in the first layer whose Fourier support contains ξ.

4 SPACE-FREQUENCY LOCALIZATION

Strong localization in both space and Fourier domains is a highly desirable property in classical signal processing which is known to be critical for robust signal approximations and reconstructions (Donoho et al., 1998). In a nutshell, localization entails that the energy of a signal is highly localized, so that complex information can be efficiently decomposed into well localized components. Emerging evidence shows that space-frequency localization of the activation function is equally important in INRs.

For this reason, the selection of PSWFs in the PIN design has a major impact to explain their excellent performnance. The visualization in figure 1 illustrates the behavior of PSWFs across space and Fourier domains. In the spatial domain, we can observe how PSWF is highly localized within a specific region, rapidly tapering off away from the center. This localization is mirrored in the frequency domain, where the function is confined within a finite bandwidth. In section 5 we prove that the output of PIN $\Phi_\theta(\boldsymbol{r})$ is a polynomial of PSWF with a degree of K^{L-1}. Moreover, the Fourier transform of $\Phi_\theta(\boldsymbol{r})$ is band-limited and with rapid space decay which contributes to the advantage in INRs.

5 LOCALIZATION AND EXPRESSIVITY PROPERTIES OF PIN

Our INR architectures can be decomposed into a mapping function $\gamma(\boldsymbol{r}) : \mathbb{R}^d \to \mathbb{R}^{T_0}$, also called positional encoding, followed by an MLP with weights $\boldsymbol{W}_k \in \mathbb{R}^{T_k \times T_{k-1}}$, biases $\boldsymbol{b}_k \in \mathbb{R}^{T_k}$ and activation function ρ applied elementwise. By denoting as $\boldsymbol{z}_k$ the post-activation functions, the INR computes the output function $\Phi_\theta = \boldsymbol{z}_L$ as form equation 1. Our PIN adopts the PSWFs, denoted below with the symbol ψ, as the activation function ($\rho = \psi$). We choose ψ to be the PSWF of order 0.

Theorem 1. *Let $\Phi_{\boldsymbol{\theta}}(\mathbf{r}) : \mathbb{R}^d \to \mathbb{R}$ be an L layer PIN, with weights $\boldsymbol{W}_k \in \mathbb{R}^{T_k \times T_{k-1}}$, biases $\boldsymbol{b}_k \in \mathbb{R}^{T_k}$ in k-th layer, assume the activation function ψ is PSWF which can be approximated with a polynomial of degree at most K, that is $\psi(x) = \sum_{m=0}^{K} \alpha_m x^m$.*

Then, $\Phi_{\boldsymbol{\theta}}(\mathbf{r})$ can be expressed as polynomial of $\psi(\boldsymbol{W}_1^{(t)} \gamma(\boldsymbol{r}) + b_t)$ with degree at most K^{L-1}

$$\Phi_{\boldsymbol{\theta}}(\mathbf{r}) = \sum_{m=0}^{K^{L-1}} \sum_{\ell_1+\ell_2+\cdots\ell_n=m} \prod_{t=1}^{n} \hat{\alpha}_{\ell_t} \left(\psi(\boldsymbol{W}_1^{(t)} \gamma(\boldsymbol{r}) + b_t)\right)^{\ell_t}.$$

Theorem 1 shows that the Fourier transform of $\Phi_{\boldsymbol{\theta}}(\mathbf{r})$ is a K^{L-1}-order convolution of Fourier transforms of PSWFs ψ. Since ψ is band-limited, and the convolution of band-limited functions is band-limited, then $\Phi_{\boldsymbol{\theta}}(\mathbf{r})$ is also band-limited. Additionally, since convolution increases regularity, $\Phi_{\boldsymbol{\theta}}(\mathbf{r})$ has high-order of regularity in the Fourier domain implying that $\Phi_{\boldsymbol{\theta}}(\mathbf{r})$ has very rapid decay in space, that is it is highly localized.

6 ADAPTIVE ACTIVATION FUNCTION PARAMETERS LEARNING

We have argued above that the optimal spatial and frequency concentration of PSWF positively impacts the performance of the INR model. Another critical advantage of this approach is its flexibility to determine the best hyperparameters of the PSWF activation.

As noted above, the parameters of activation functions in WIRE and GAUSS are chosen ad-hoc for different tasks and different signals using a grid search (Saragadam et al., 2023). However, the activation function's parameters resulting from such a grid search are local. i.e., *they are only optimal*

for the signal that has been used in the grid search, while they are suboptimal for other signals, affecting the expressivity of the INR model. Even if those parameters are designed to be learnable, the initialization still impacts the parameters of the learned activation function. For instance, the parameters in the Gabor wavelet $\psi\left(x;\omega,s\right)=e^{j\omega x}e^{-|sx|^2}$ are ω and s, representing the frequency and scale respectively; in Gaussian function $\psi\left(x;s\right)=e^{-(sx)^2}$, the parameter s represents the scale. As the parameters of these functions appear in an exponent, it is difficult to learn wider frequency or scale distributions.

The situation is different for our PSWF activations as we do not use an explicit formulation, but we use a numerical approximation, so there are no explicit parameters to control. Rather, we apply an indirect way to control the amplitude, frequency, and height characteristics of the PSWF. That is, for the predefined PSWF function $\psi(x)$, we instantiate the learnable PWSF activation function by $\hat{\psi}(x)=T\,\psi(wx)+b$. In this case, the amplitude, frequency, and height of the PSWF activation function are indirectly controlled by T, w, and b, respectively. The construction of PSWFs as an activation, detailed explanations and ablations on adaptive activation function parameter learning are provided in section A.1 in Appendix.

7 Experiments

7.1 Image representation

Image representation, commonly referred to as image regression, is a measure that evaluates the expressive capabilities of INRs. A superior INR should not only represent the original signal but also preserve a substantial amount of the structural information, texture, color, and contrast of the image. For assessing the effectiveness of INRs in image representation tasks, the Kodak Lossless True Color Image Dataset (Franzen, 1999) was employed. This dataset was chosen to analyze the performance of the PIN across a comprehensive set of images rather than limiting the evaluation to a single example. Comprising 24 images with varied spatial and frequency content, the dataset presents a robust challenge, requiring the PIN to maintain high fidelity in representation. PIN was subsequently trained on each image in the dataset. The left panel of figure 2 showcases the 15^{th} image from the dataset alongside the image representations generated by various INRs. On the right of the same figure displays the variation in PSNR across the dataset for different INRs, where each image is indexed along the circumference of the radar plot. The PSNR values for PIN are highlighted in black.

The child image on the left of figure 2 showcases the PIN's color accuracy and its capability of extracting highly varying contents of the image into the weights and biases of an INR compared to existing INRs. A closer look at the decoded representations of the existing baselines reveals that INRs which are only frequency-compact, like SIREN, tend towards a low-pass representation of the explicit representation, failing to capture intricate details. On the other hand, INRs that are both space-frequency compact but with rapid decay in both domains showcase the ability to capture fast-varying components of images into the INR. However, when they focus more on finer details, they fail to balance smooth regions, introducing some additional noise. As PSWFs are the optimal representation in both domains, PIN focuses on both finer and smooth regions, encoding the signal optimally with minimal distortion. Due to PIN's ability to effectively focus on both high and low-frequency components, it outperforms the existing baselines across all images in the dataset, consistently delivering a PSNR of at least 30 dB. Additional image representation results including a thorough evaluation on DIV2K dataset (Agustsson & Timofte, 2017), and learning curves are provided in the supplementary material.

7.2 Solving the wide frequency spectrum challenge via PIN

Even though INRs are proficient at converting explicit signals to implicit representations, their performance is impeded when dealing with signals that encompass a wide frequency spectrum. Specifically, while INRs that incorporate Fourier feature encodings (Landgraf et al., 2022) excel at capturing fine details through high-frequency components, they simultaneously introduce undesirable noisy elements in areas that should remain smooth. Notably, according to the findings in (Landgraf et al., 2022), SIREN (Sitzmann et al., 2020) also exhibits this limitation, struggling to maintain fi-

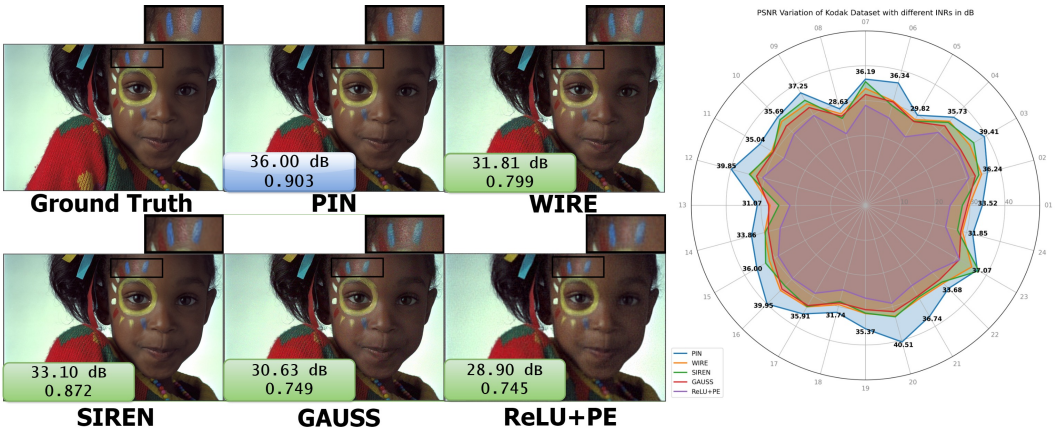

Figure 2: **Image representation capacity of PIN**: The left image shows an instance of PIN's representation capacity, and the right image shows the PIN's representation capacity evaluated on all Kodak lossless true color images. PIN stands out as the INR that achieves the highest PSNR and SSIM metrics, indicating minimal distortion and maximum preservation of structural information.

delity in smoother regions while effectively representing finer textures, and (Landgraf et al., 2022) presents a hierarchical representational approach to resolve this issue. Further, rapid decaying space-frequency non-linearities such as Gabor Wavelet (Saragadam et al., 2022) and GAUSS (Ramasinghe & Lucey, 2022) are good at focusing on fast varying components of images and capturing them efficiently into weights and biases, but when they focus on intricate details, they lose their focus on smooth regions and introduce some form of noisy component (see figure 3). However, as PSWFs are known for being optimally space and band-limited, they excel in the preservation of energy concentration. This characteristic allows them to adeptly represent finer details without encountering this issue. Therefore, PIN achieves an optimal representation that maintains high fidelity across different textural features. This effect is illustrated in figure 3, where the efficacy of PSWFs in balancing detail and smoothness is visually demonstrated compared to the existing INRs. Furthermore, this issue can be seen in the decoded representations of the child image in figure 2 as well. Therefore, from the presented visual results, it can be clearly seen that without the need for any additional architectural changes to INRs, PIN can resolve this wide frequency spectrum challenge.

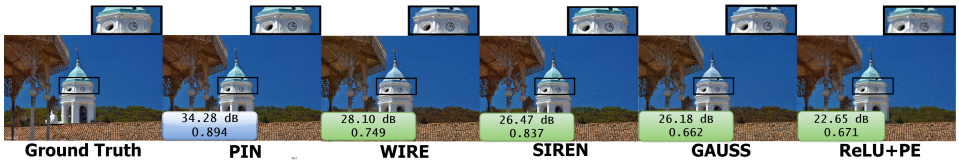

Figure 3: **Wide-Frequency spectrum challenge**: Existing INRs often attempt to emphasize finer details while not focusing much on smoother regions. This can be attributed to their nonlinearities' space-frequency trade-offs. By contrast, PINs exhibit optimal energy concentration for a given band, enabling them to effectively encode both fine details and smooth regions.

7.3 Occupancy field representation

When it comes to representing three dimensional occupancy fields, the topic of image representation, as explored in figure 2 extends into the realm of three-dimensional spaces. This extension allows for an examination of the capability of INRs to depict three-dimensional signed distance fields. In this context, the transformation occurs from a three-dimensional domain to a binary signal space, marked by the values 1 or 0. Where, a value of 1 signifies the presence of the signal within a predefined area, whereas a value of 0 denotes its absence from that area. For this experiment two occupancy volumes namely Asian Dragon, and Armadillo, which are shown in figure 4, were obtained from Stanford 3D shape dataset (Stanford University Computer Graphics Laboratory), and sampled on a grid of $512 \times 512 \times 512$, assigning a value of 1 to each voxel inside the volume and a value of 0 to those outside. The methodology for this study was derived from the work mentioned

in Saragadam et al. (2023). The obtained results are shown in figure 4 . It can be observed that in both the instances PIN effectively encode the rapidly changing three-dimensional structure into its neural representation. In contrast, when examining the performance of WIRE and SIREN, it is evident that these architectures struggle to incorporate the quickly varying components of the structure into their weights and biases, resulting in a representation that primarily captures lower frequency components. While GAUSS activation function achieves performance metrics similar to PIN, a detailed examination of the three-dimensional statues decoded from Gauss reveals distortions in some uniform areas in both instances. Conversely, PIN encodes the structure accurately without introducing any additional artifacts. Furthermore, PIN's performance has been evaluated on additional 3D shapes, and the obtained IoU values are provided in the Appendix.

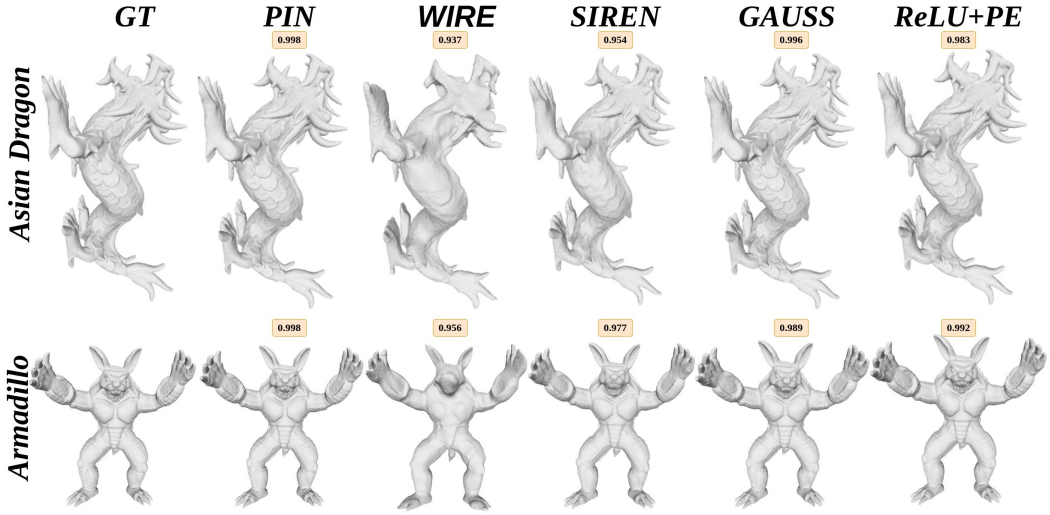

Figure 4: **Occupancy fields representation capacity of PIN**: PIN stands out as the INR that exhibits the highest similarity to the ground truth occupancy field. Unlike other INRs, the PIN approach does not converge to a low-pass representation; rather, it accurately preserves high-frequency components throughout the training process. This characteristic enables PIN to faithfully capture intricate details, making it particularly adept for tasks requiring accurate representation of complex occupancy patterns.

7.4 IMAGE INPAINTING

INRs are often employed to learn continuous functions from discretized signals. Once an INR is adequately trained, it should demonstrate excellent generalization capabilities even with limited training samples. A notable application in computer vision is image inpainting. In this approach, during the training phase, an INR receives partial data from an image. In the testing phase, the INR is tasked with reconstructing the missing positions of the image. Image inpainting is a measure to determine if the learned underlying representation has overfitted to the provided training data.

We employ two testing strategies: one involves training with 70% of the data sampled randomly, and the other uses a predefined text mask that obscures the image with varying font sizes. The top row of the figure 5 shows inpainting results, corresponding to 70% random sampling, whereas the bottom of the same figure shows the text-masked inapinting results. In both instances the second column represents the masked image. As can be clearly seen from the results, PIN is the only architecture that maintains the highest PSNR and SSIM values in both instances, indicating superior recovery capabilities with minimal distortion and the highest structural similarity to the original image. Additionally, it is the architecture that produced the most visually appealing reconstruction in comparison with the ground truth.

When comparing the performance of various INRs, it is evident that WIRE exhibits signs of overfitting to the training data and has not generalized well. SIREN demonstrates commendable generalization capabilities within the context of INRs, yet it is constrained by its need for highly specific weight initialization and frequency parameters. In contrast, PIN operates without such stringent re-

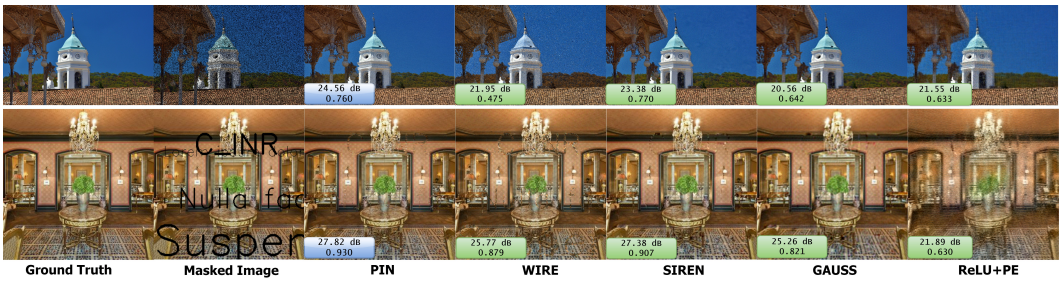

Figure 5: **Image Inpainting Capabilities of PIN**: Among the existing INRs, PIN stands out as the top image inpainting performer, excelling not only in achieving the highest PSNR in both instances, but also in generating the inpainting results most visually similar to the ground truth. PIN's superior metrics highlight its proficiency in restoring images with minimal distortion while preserving maximum structural information.

quirements and consistently delivers superior performance. Therefore, PIN is particularly effective for image inpainting, producing visually appealing results even when reconstructing highly obscured images. This underscores its robust generalization ability compared to existing compactly supported INRs like WIRE and GAUSS, and sets a new benchmark that surpasses current state-of-the-art methods.

7.5 Neural Radiance Fields

The core area benefiting from INRs is NeRFs (Mildenhall et al., 2020). In NeRF, a scene is encoded into an INR by feeding the viewer's coordinates (x, y, z) and the viewing directions (θ, ϕ) into the INR. The INR is tasked with predicting the corresponding location's color and density. When the INR is well-trained, it gains the ability to generate novel views from different spatial locations and viewing angles, those are not included in the training data. This remarkable capability is achieved by training a 3D implicit function using spatial coordinates (x, y, z) and viewing directions (θ, ϕ) allowing for the synthesis of highly realistic images and scenes. For this experiment, we used a vanilla NeRF architecture consisting of two fully connected blocks, each containing four layers, and the drums dataset with 100 training images and 200 testing images. One of the obtained novel views for each INR is presented in figure 6. PIN's remarkable performance can be attributed to its optimal energy concentration within a specified frequency band, distinguishing it from other methods and reinforcing its superiority. Additional novel views are provided in the supplementary material.

Figure 6: **Novel View Synthesis Capabilities of PIN**: PIN achieves the highest PSNR in novel views performance as compared to existing INRs. While existing INRs tend to produce blurry novel views in feature-dense areas, PIN's ability to preserve maximum energy in a given state allows it to encode intricate details into its weights and biases, and produce novel views that exhibit the highest similarity to the ground truth.

7.6 Ablation Study

7.6.1 Network Hyperparameters

An ablation study was conducted to evaluate the effectiveness of PINs with various hyperparameters selected during the training environment. For this experiment, we used the child image shown in figure 2. This hyperparameter tuning included the variation of PSNR with the number of hidden

neurons, while keeping the number of hidden layers constant at 3 (shown in the left figure of figure 7). Additionally, the study examined the variation of PSNR with the number of hidden layers, while maintaining the number of hidden neurons at 300 (shown in the middle figure of figure 7). Lastly, the variation of PSNR with the learning rate was analyzed, with the number of hidden layers kept at 3 and the number of hidden neurons at 300 (shown in the right figure of figure 7)

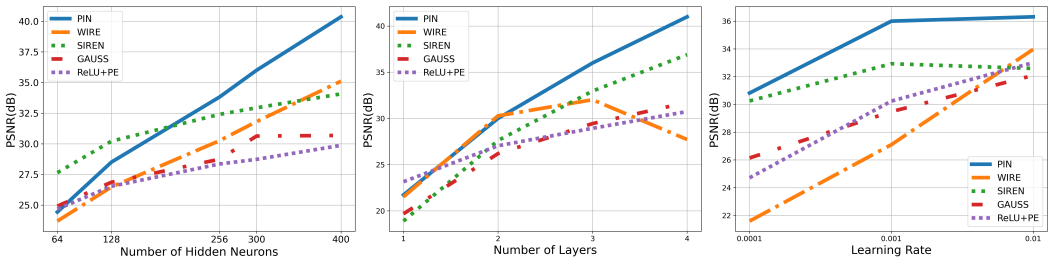

Figure 7: **Hyperparameter Turning of PIN**: PIN demonstrates a sharp linear increase in PSNR with the addition of more hidden neurons and layers compared to existing INRs. Instead of becoming unstable with higher learning rates, PIN stabilizes its PSNR, maintaining nearly constant performance.

In general, increasing the number of hidden neurons or hidden layers in an INR enhances its capacity due to the higher number of learnable parameters. As shown in the left and middle plots of figure 7, PIN exhibits an approximately linear increase, with a higher gradient compared to other INRs, in PSNR with the addition of more hidden neurons and hidden layers. However, as the learning rate increases, PIN demonstrates PSNR saturation effects instead of tending toward instability, as illustrated in the right plot of figure 7.

7.7 Theoretical analysis, ablation studies, and additional experiments

In the appendix, we provide a comprehensive theoretical analysis of PIN's forward propagation, alongside a combined theoretical and experimental investigation into why existing baseline space-frequency compact INRs fall short compared to PIN. This analysis helps to elucidate the superior performance of PIN in capturing complex details. The appendix also includes the complete numerical implementation of PIN, where we demonstrate its robustness to variations in parameters and provide a detailed examination of how different weight initialization strategies impact its performance. Furthermore, we showcase PIN's learning curves and extensive experimental results to support the findings presented in the main sections. In addition to these results, the appendix features further analysis of PIN's capabilities through a set of additional experiments. These experiments explore PIN's ability to handle high-frequency encoding, perform effective image denoising, and detect edges with precision.

8 Conclusion

Implicit Neural Representations (INRs) have emerged as a very promising framework in computer vision and image processing, yet their performance is very sensitive on the choice of activation functions. Empirical results indicate that well-localized activation functions with good space-frequency concentration are more effective than sinusoidal functions which suffer from poor spatial decay. For instance, current INRs often focus more on encoding intricate details into weights and biases of the INR, and do not handle well smoother regions. Further, they underperform in reconstructing sparse or noisy data due to overfitting. To overcome these limitations, we propose the use of PSWF as activation function for INRs. PSWFs maximize joint space-frequency domain concentration, a crucial feature for enhancing INR capabilities. Our numerical experiments demonstrate that INRs with PSWF activations significantly improve expressivity and generalizability, boosting performance across various tasks including image and 3D shape representation, novel view synthesis, reconstruction from sparse or noisy measurements,and edge detection.

REFERENCES

Eirikur Agustsson and Radu Timofte. Ntire 2017 challenge on single image super-resolution: Dataset and study. In *The IEEE Conference on Computer Vision and Pattern Recognition (CVPR) Workshops*, July 2017.

Jonathan T Barron, Ben Mildenhall, Matthew Tancik, Peter Hedman, Ricardo Martin-Brualla, and Pratul P Srinivasan. Mip-nerf: A multiscale representation for anti-aliasing neural radiance fields. In *2021 IEEE/CVF International Conference on Computer Vision (ICCV)*, pp. 5835–5844. IEEE, 2021.

Ronen Basri, Meirav Galun, Amnon Geifman, David Jacobs, Yoni Kasten, and Shira Kritchman. Frequency bias in neural networks for input of non-uniform density. In *International Conference on Machine Learning*, pp. 685–694. PMLR, 2020.

Henry A Brown and NAVAL RESEARCH LAB WASHINGTON DC. *Image Enhancement with Prolate Spheroidal Wave Functions*. Naval Research Laboratory, 1968.

Yuan Cao, Zhiying Fang, Yue Wu, Ding-Xuan Zhou, and Quanquan Gu. Towards understanding the spectral bias of deep learning. *arXiv preprint arXiv:1912.01198*, 2019.

Anpei Chen, Zexiang Xu, Xinyue Wei, Siyu Tang, Hao Su, and Andreas Geiger. Factor fields: A unified framework for neural fields and beyond. *arXiv preprint arXiv:2302.01226*, 2023a.

Zhang Chen, Zhong Li, Liangchen Song, Lele Chen, Jingyi Yu, Junsong Yuan, and Yi Xu. Neurbf: A neural fields representation with adaptive radial basis functions. In *CVPR*, pp. 4182–4194, 2023b.

Mikolaj Czerkawski, Javier Cardona, Robert Atkinson, Craig Michie, Ivan Andonovic, Carmine Clemente, and Christos Tachtatzis. Neural knitworks: Patched neural implicit representation networks. *arXiv preprint arXiv:2109.14406*, 2021.

David L. Donoho, Martin Vetterli, Ronald A. DeVore, and Ingrid Daubechies. Data compression and harmonic analysis. *IEEE transactions on information theory*, 44(6):2435–2476, 1998.

Rich Franzen. Kodak lossless true color image suite. `https://r0k.us/graphics/kodak/`, 1999. Accessed on May 21, 2024.

Laurent Gosse. Compressed sensing with preconditioning for sparse recovery with subsampled matrices of slepian prolate functions. *Annali dell'Universita' di Ferrara*, 59:81–116, 2013.

Jeffrey A Hogan, Scott Izu, and Joseph D Lakey. Sampling approximations for time-and bandlimiting. *Sampling Theory in Signal and Image Processing*, 9:91–117, 2010.

Nan Hu, Xu Xu, and Zhongfu Ye. Doa estimation for wideband signals based on sparse signal reconstruction using prolate spheroidal wave functions. *Signal processing*, 96:395–400, 2014.

Arthur Jacot, Franck Gabriel, and Clément Hongler. Neural tangent kernel: Convergence and generalization in neural networks. *Advances in neural information processing systems*, 31, 2018.

Amirhossein Kazerouni, Reza Azad, Alireza Hosseini, Dorit Merhof, and Ulas Bagci. Incode: Implicit neural conditioning with prior knowledge embeddings. In *Proceedings of the IEEE/CVF Winter Conference on Applications of Computer Vision*, pp. 1298–1307, 2024.

Kedar Khare and Nicholas George. Sampling theory approach to prolate spheroidal wavefunctions. *Journal of Physics A: Mathematical and General*, 36(39):10011, 2003.

Henry J Landau and Henry O Pollak. Prolate spheroidal wave functions, fourier analysis and uncertainty—ii. *Bell System Technical Journal*, 40(1):65–84, 1961a.

Henry J Landau and Henry O Pollak. Prolate spheroidal wave functions, fourier analysis and uncertainty—ii. *Bell System Technical Journal*, 40(1):65–84, 1961b.

Henry J Landau and Henry O Pollak. Prolate spheroidal wave functions, fourier analysis and uncertainty—iii: the dimension of the space of essentially time-and band-limited signals. *Bell System Technical Journal*, 41(4):1295–1336, 1962.

Zoe Landgraf, Alexander Sorkine Hornung, and Ricardo Silveira Cabral. Pins: progressive implicit networks for multi-scale neural representations. *arXiv preprint arXiv:2202.04713*, 2022.

Martin A Lindquist. Optimal data acquisition in fmri using prolate spheroidal wave functions. *International Journal of Imaging Systems and Technology*, 13(2):126–132, 2003.

Martin A Lindquist and Tor D Wager. Spatial smoothing in fmri using prolate spheroidal wave functions. *Human Brain Mapping*, 29(11):1276–1287, 2008.

Zhen Liu, Hao Zhu, Qi Zhang, Jingde Fu, Weibing Deng, Zhan Ma, Yanwen Guo, and Xun Cao. Finer: Flexible spectral-bias tuning in implicit neural representation by variable-periodic activation functions. In *Proceedings of the IEEE/CVF Conference on Computer Vision and Pattern Recognition*, pp. 2713–2722, 2024.

Julien NP Martel, David B Lindell, Connor Z Lin, Eric R Chan, Marco Monteiro, and Gordon Wetzstein. Acorn: adaptive coordinate networks for neural scene representation. *ACM Transactions on Graphics (TOG)*, 40(4):1–13, 2021.

Lars Mescheder, Michael Oechsle, Michael Niemeyer, Sebastian Nowozin, and Andreas Geiger. Occupancy networks: Learning 3d reconstruction in function space. In *Proceedings of the IEEE/CVF conference on computer vision and pattern recognition*, pp. 4460–4470, 2019.

B Mildenhall, PP Srinivasan, M Tancik, JT Barron, R Ramamoorthi, and R Ng. Nerf: Representing scenes as neural radiance fields for view synthesis. In *European conference on computer vision*, 2020.

Ian C Moore and Michael Cada. Prolate spheroidal wave functions, an introduction to the slepian series and its properties. *Applied and Computational Harmonic Analysis*, 16(3):208–230, 2004.

Michael Niemeyer, Lars Mescheder, Michael Oechsle, and Andreas Geiger. Differentiable volumetric rendering: Learning implicit 3d representations without 3d supervision. In *Proceedings of the IEEE/CVF Conference on Computer Vision and Pattern Recognition*, pp. 3504–3515, 2020.

Andrei Osipov, Vladimir Rokhlin, Hong Xiao, et al. Prolate spheroidal wave functions of order zero. *Springer Ser. Appl. Math. Sci*, 187, 2013.

Jeong Joon Park, Peter Florence, Julian Straub, Richard Newcombe, and Steven Lovegrove. Deepsdf: Learning continuous signed distance functions for shape representation. In *Proceedings of the IEEE/CVF conference on computer vision and pattern recognition*, pp. 165–174, 2019.

Nasim Rahaman, Aristide Baratin, Devansh Arpit, Felix Draxler, Min Lin, Fred Hamprecht, Yoshua Bengio, and Aaron Courville. On the spectral bias of neural networks. In *International Conference on Machine Learning*, pp. 5301–5310. PMLR, 2019.

Sameera Ramasinghe and Simon Lucey. Beyond periodicity: Towards a unifying framework for activations in coordinate-mlps. In *European Conference on Computer Vision*, pp. 142–158. Springer, 2022.

Christian Reiser, Songyou Peng, Yiyi Liao, and Andreas Geiger. Kilonerf: Speeding up neural radiance fields with thousands of tiny mlps. In *Proceedings of the IEEE/CVF International Conference on Computer Vision*, pp. 14335–14345, 2021.

T Mitchell Roddenberry, Vishwanath Saragadam, Maarten V de Hoop, and Richard G Baraniuk. Implicit neural representations and the algebra of complex wavelets. *arXiv preprint arXiv:2310.00545*, 2023.

Vishwanath Saragadam, Jasper Tan, Guha Balakrishnan, Richard G Baraniuk, and Ashok Veeraraghavan. Miner: Multiscale implicit neural representation. In *ECCV*, pp. 318–333. Springer, 2022.

Vishwanath Saragadam, Daniel LeJeune, Jasper Tan, Guha Balakrishnan, Ashok Veeraraghavan, and Richard G Baraniuk. Wire: Wavelet implicit neural representations. In *CVPR*, pp. 18507–18516, 2023.

Liyue Shen, John Pauly, and Lei Xing. Nerp: implicit neural representation learning with prior embedding for sparsely sampled image reconstruction. *IEEE Transactions on Neural Networks and Learning Systems*, 2022.

Kexuan Shi, Xingyu Zhou, and Shuhang Gu. Improved implicit neural representation with fourier reparameterized training. *arXiv preprint arXiv:2401.07402*, 2024.

Vincent Sitzmann, Julien Martel, Alexander Bergman, David Lindell, and Gordon Wetzstein. Implicit neural representations with periodic activation functions. *NeurIPS*, 33:7462–7473, 2020.

David Slepian. Prolate spheroidal wave functions, fourier analysis and uncertainty—iv: extensions to many dimensions; generalized prolate spheroidal functions. *Bell System Technical Journal*, 43 (6):3009–3057, 1964.

David Slepian and Henry O Pollak. Prolate spheroidal wave functions, fourier analysis and uncertainty—i. *Bell System Technical Journal*, 40(1):43–63, 1961.

Stanford University Computer Graphics Laboratory. The stanford 3d scanning repository. `https://graphics.stanford.edu/data/3Dscanrep/`. Accessed: 2024-07-15.

Yu Sun, Jiaming Liu, Mingyang Xie, Brendt Wohlberg, and Ulugbek S Kamilov. Coil: Coordinate-based internal learning for tomographic imaging. *IEEE Transactions on Computational Imaging*, 7:1400–1412, 2021.

Matthew Tancik, Pratul Srinivasan, Ben Mildenhall, Sara Fridovich-Keil, Nithin Raghavan, Utkarsh Singhal, Ravi Ramamoorthi, Jonathan Barron, and Ren Ng. Fourier features let networks learn high frequency functions in low dimensional domains. *Advances in Neural Information Processing Systems*, 33:7537–7547, 2020.

Peihao Wang, Zhiwen Fan, Tianlong Chen, and Zhangyang Wang. Neural implicit dictionary learning via mixture-of-expert training. In *International Conference on Machine Learning*, pp. 22613–22624. PMLR, 2022.

Herwig Wendt, Maarten V de Hoop, Fredrik Andersson, and Anton Duchkov. Multi-scale structured imaging using wave packets and prolate spheroidal wave functions. In *SEG International Exposition and Annual Meeting*, pp. SEG–2010. SEG, 2010.

Gizem Yüce, Guillermo Ortiz-Jiménez, Beril Besbinar, and Pascal Frossard. A structured dictionary perspective on implicit neural representations. In *Proceedings of the IEEE/CVF Conference on Computer Vision and Pattern Recognition*, pp. 19228–19238, 2022.